JOURNAL OF MATERIALS SCIENCE 21 (1986) 2257–2263

High temperature deformation of Mn–Zn ferrite single crystals

M. UEMURA
Department of Energy Engineering, Toyohashi University of Technology, Toyohashi 440, Japan

T. HYONO
Materials and Electronic Devices Laboratory, Mitsubishi Electric Corp., Amagasaki 661, Japan

M. UMENO, H. KAWABE
Department of Precision Engineering, Osaka University, Suita 565, Japan

Compressive creep tests in a temperature region higher than 900° C were conducted on Mn–Zn ferrite single crystals of various compositions. The strain rates in the stationary creep vary with stress and temperature according to the well-known relation

$$\dot{\varepsilon} = A\sigma^m \exp(-H/kT)$$

The stress index, m, is nearly 3, independent of the composition, but the activation energy, H, depends on it. From TEM and etch pit observations the distribution of mobile dislocations were almost uniform and the effective stress index, m^*, of the dislocation velocity was nearly 1. In the compression test with constant deformation velocity, the internal stress during the deformation was about 17% lower than the applied stress. From these experimental results the high temperature deformation of Mn–Zn ferrite crystals is concluded to be governed by the viscous movements of dislocations which drag the atmosphere of pinning atoms or ions. The chemical composition dependency of the activation energy is considered to be caused by the structural defects due to the deviation from stoichiometry which act as the obstacles for the diffusion of pinning atoms or ions.

1. Introduction

Some physical properties of crystals having the spinel structure depend on their chemical compositions, that is on their deviation parameters, n (n being 1 in stoichiometric composition). The mechanical properties of these crystals have been studied mainly on spinel crystals ($MgO \cdot nAl_2O_3$, $1 \leqslant n \lesssim 4.5$) in relation to their chemical compositions. The high temperature strength of the spinel crystals decreases with the deviation from the stoichiometry [1–3], while the activation energy of deformation is almost constant [3]. By transmission electron microscope (TEM) observations, mobile dislocations in spinel crystals separate into two collinear half-dislocations having the Burgers vector of $(a/4)\langle 1\,1\,0\rangle$ and the separation does not occur in the slip plane [1, 3–7]. Some models of the dislocation splitting and high temperature deformation have been presented [1, 3, 7], but these could not explain many experimental results comprehensively. The plastic deformation behaviour of Mn–Zn ferrite crystals, having the spinel structure is not known well.

In the study of creep deformations of metals and alloys, the high temperature stationary deformation is classified into two types [8]:

1. Deformation rate is governed by recovery, as is seen mostly in pure metals (the metal type), and
2. it is governed by the viscous movement of dislocations dragging the atmosphere of impurity atoms, as is observed in alloys (the alloy type).

Knowing some deformation parameters, the type of deformation mode is determined. In the metal type the dislocation configuration is not uniform and some cell and sub-grain structures are existing [9], and the recovery due to the climb motion of dislocations at the cell walls and sub-grain boundaries [10], or that due to the growth of dislocation networks [11], governs the dislocation velocity. In this case the stress index, m, of the strain rate becomes larger than 5 and the internal stress becomes high [12, 13]. In the alloy type the distribution of dislocations is nearly uniform [14], the stress index is nearly 3 [15], the internal stress is low and the effective stress index, m, of dislocation velocity is almost unity. The classification of deformation mechanism by these deformation parameters is used in many materials.

In the present work high temperature deformation of Mn–Zn ferrite single crystals is studied by compressive creep and by constant speed deformation test, and the type of deformation mechanism is determined from the deformation parameters and dislocation configurations observed by TEM and etch pit method.

0022–2461/86 $03.00 + .12

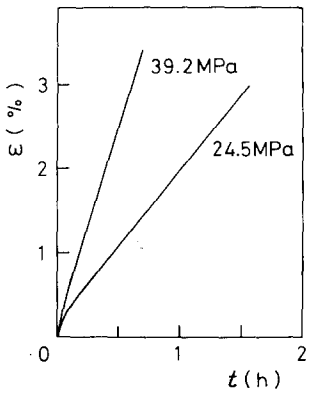

Figure 1 Creep curves of an Mn–Zn ferrite crystal with $n = 1.13$. The compression direction is [0 1 1].

2. Experimental details

The specimens for compression test were cut out from Bridgman grown Mn–Zn ferrite single crystals having various compositions of $(MnO)_x \cdot (ZnO)_{1-x} \cdot n(Fe_2O_3)$ with $0.47 \leqslant x \leqslant 0.65$ and $1.02 \leqslant n \leqslant 1.86$ by atomic absorption spectroscopy. The specimens are parallelepipeds of $3.5 \times 3.5 \times 10\,mm^3$ with [0 0 1] or [0 1 1] compression axes. The specimen surface, i.e. flanks of the parallelepipeds, were ground with No. 1500 emery paper and No. 2000 alumina powder to elimate the damaged surface layer. The creep test was conducted in an open furnace applying a load with a pair of alumina rods between which the specimen was held. The strain of the specimen was measured by a differential transformer. To prevent the chemical reaction of the specimen and the alumina rods during the compression at a high temperature, a Pt sheet of 20 μm thick was inserted between them. The constant speed compression test was done in an argon atmosphere at 1100° C using an image furnace installed to an Instron machine (TTCM-L). The deformed specimens were investigated with TEM and etch pit method. The foils for TEM observation were made by ion-beam thinning and the high voltage electron microscope HU-3000 in the Center for Ultra High Voltage Electron Microscopy of Osaka University was utilized at the operating voltage of 2000 kV. Etch pits were obtained with thermal phosphoric acid [16] or 10% H_2SO_4 + Zn powder [17] according to the chemical composition of the specimen.

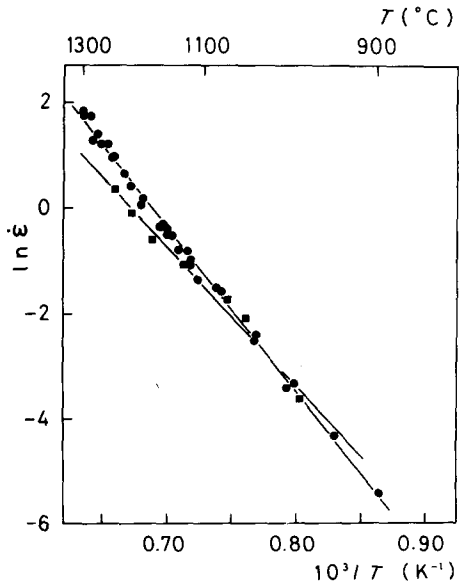

Figure 2 Arrhenius plots of strain rate of [0 1 1] compressive creep, $P = 26.7$ MPa. The activation energies, H, obtained are also shown. (■) $n = 1.02$, $H = 2.29$ eV, (●) $n = 1.13$, $H = 2.71$ eV.

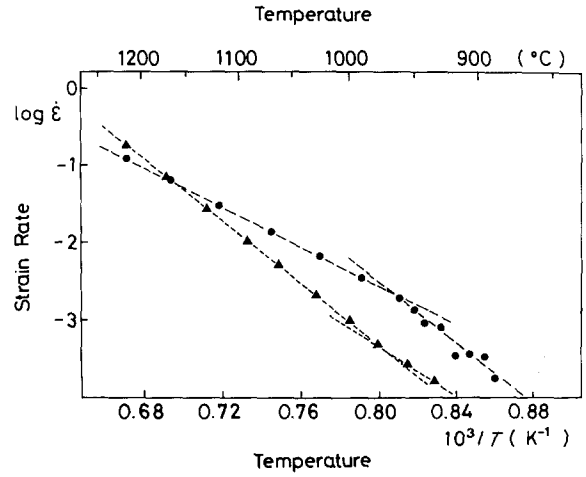

Figure 3 Arrhenius plots of strain rate of [0 0 1] compressive creep of nearly stoichiometric and non-stoichiometric crystals, $P = 34.3$ MPa. Note that both lines bend nearly at 1000° C. (●) $n = 1.05$, (▲) $n = 1.57$.

3. Experimental results

3.1. Activation energy

Fig. 1 shows the creep curve of a crystal with the composition ratio of $n = 1.13$ for the compression direction [0 1 1] at 1252° C. Transtition creep appears just after the loading and the stationary creep begins at $\varepsilon = (L_0 - L)/L_0 \simeq 0.5\%$. The creep natures of other crystals and/or other creep conditions are nearly the same. The strain rate $\dot{\varepsilon}$ in the stationary creep satisfies the well-known relation

$$\dot{\varepsilon} = A\sigma^m \exp(-H/kT) \qquad (1)$$

where σ, m and H are applied stress, stress index and activation energy, respectively. The stress index and the activation energy were determined for crystals of various compositions from the strain rate of stationary creep. Figs. 2 and 3 show the Arrhenius plots of the strain rates of the crystals for compressions along [0 1 1] and [0 0 1], respectively. The activation energies

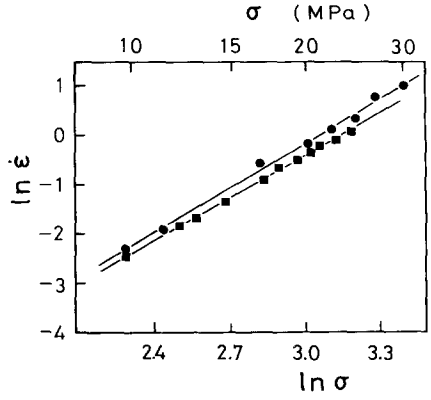

Figure 4 Stress dependencies of strain rates of two crystals. The stress indices, m, are nearly 3 for both crystals. (●) $n = 1.02$ [0 1 1] 1247° C, $m = 2.99$; (■) $n = 1.13$ [0 1 1] 1262° C, $m = 2.88$.

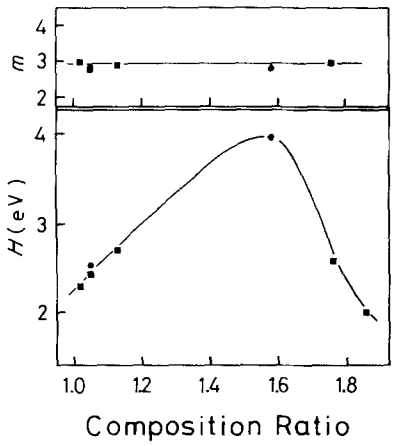

Figure 5 Activation energies and stress indices for the Mn–Zn ferrites of various chemical compositions. (●) [0 0 1], (■) [0 1 1].

obtained from the inclination of the curves are also shown. In Fig. 3 the inclinations of both curves change nearly at 1000° C, and for $n = 1.57$ [0 0 1] the activation energy is as high as about 4 eV at temperatures higher than 1000° C. The deformation behaviour in the lower temperature region will be discussed later. Fig. 4 shows the stress – strain rate relations of the crystals with $n = 1.02$ and 1.13. The stress indices, m, obtained from the inclination of the curve are designated in the figure. The activation energies and stress indices for various compositions are shown in Fig. 5. The stress index is almost constant at nearly 3 for the crystals of various compositions, while the activation energy varies significantly. This differs greatly from spinel crystals, in which stress index is nearly 4 and the activation energy does not depend on n.

3.2. Dislocation configurations

From the stress index of $m = 3$, the deformation of Mn–Zn ferrite crystals is considered to be governed by the viscous movement of dislocations, that is alloy type or viscosity ruling. In this case dislocation configurations of deformed crystals are uniform without cell structures and sub-boundaries. Fig. 6 shows a typical TEM image of dislocations in the specimen deformed 3.38% by creep at 1100° C and cooled as loaded. Dislocations are mostly straight and uniformly distributed except the grown-in sub-boundaries.

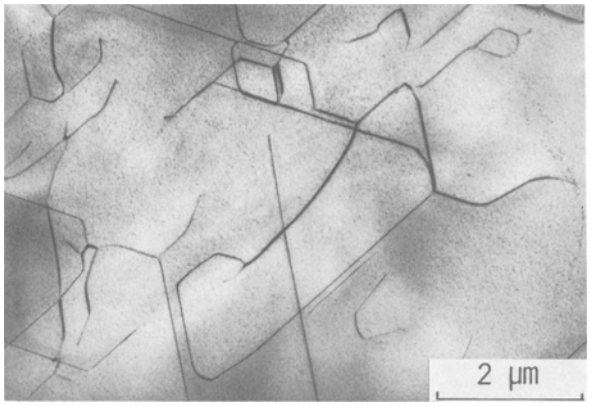

Figure 6 Dislocation network in the primary slip plane of a crystal with $n = 1.13$ deformed by compressive creep along [0 0 1] by 3.38% at 1100° C with the load of 50.2 MPa. Dislocations are almost straight along ⟨1 1 0⟩ and no cell structures are seen.

In other specimens with different compositions the dislocation configurations are nearly the same and cell structures are not formed. Extended dislocations are frequently observed as shown in Fig. 7. In Fig. 7a short segments of extended dislocations are edge type and two partial dislocations of $(a/4)\langle 1\,1\,0\rangle$ are separated by climb, and in Fig. 7b 60° dislocations extend on a non-slipping (0 1 0) plane. The separation of the partial dislocations are about 20 nm.

3.3 Etch pit observation

The macroscopic distribution of dislocations was observed by the etch pit method. A flank of the deformed specimen was lapped-off for about 1 mm and chemically polished with thermal phosphoric acid. The etch pit distributions of deformed crystals are uniform as shown in Fig. 8 except the peripheries of the specimen for any compositions and deformation conditions. By the investigation of etch pit patterns the slip system of Mn–Zn ferrite crystals is determined to be $\{1\,1\,1\}\langle 1\,\bar{1}\,0\rangle$ independent of chemical composition and deformation direction, while in spinel crystals the $\{1\,1\,0\}\langle 1\,\bar{1}\,0\rangle$ system is also activated [16].

3.4. The internal stress (σ_i)

The measurement of internal stress $\sigma_i (= \sigma - \sigma_{eff})$ during the deformation is a useful way to study the deformation mechanism, as its value is quite different between the recovery and viscosity rulings in high temperature deformation. The internal stresses are measured from the change of effective stresses, σ_{eff}, by varying strain rate or temperature keeping the internal dislocation structure unchanged. In the present work we employed the incremental unloading method using the Instron machine. In this method stepwise "unloadings" are done during the deformation and the amount of stress at $d\sigma/dt = 0$ is measured as σ_i. Fig. 9 shows the procedure of the incremental stress measurement. The specimen with $n = 1.13$ is compressed in [0 0 1] direction at 1100° C and deformation is stopped at $\varepsilon \simeq 12\%$ by unloading. At the first unloading $\dot{\sigma} = 0$ was obtained. The stress at $\dot{\sigma} = 0$ was further decreased, $\dot{\sigma}$ became positive and by the third unloading $\dot{\sigma} = 0$ was obtained. The stress as $\dot{\sigma}$ - 0 was 16.9% of the applied stress before unloading, which is rather low compared with the estimated 50% in spinel crystals. Fig. 9 shows that although the deformation rate is constant any work hardening is not seen in this deformation condition. This means that the internal dislocation structure is not changed during the test. The gradual linear increment of stress after the yield is only caused by the increase of cross-section of the specimen due to deformation and therefore the deformation behaviour is considered to be almost the same as in stationary creep.

3.5. Effective stress index (m^*)

The effective stress index, m^*, of dislocation velocities is nearly unity in the viscosity ruling. However, m^* of Mn–Zn ferrite crystal has not been measured, as the direct measurement of the dislocation velocity requires a high temperature. We estimated it from the stress

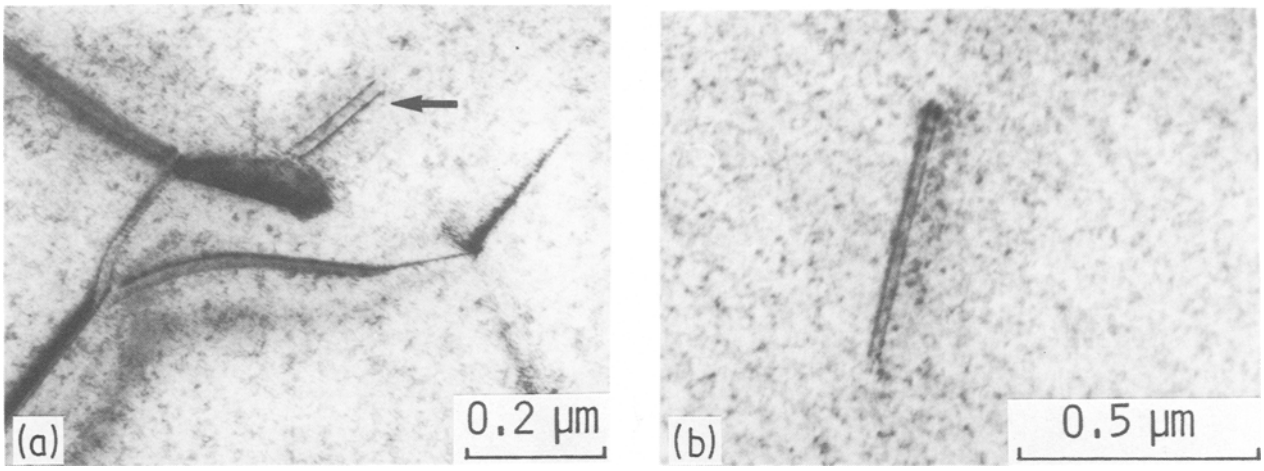

Figure 7 TEM images of extended dislocations observed in a creep-deformed specimen with $n = 1.13$ along [0 0 1]. (a) The dislocation pointed by an arrow lies on $(1\,\bar{1}\,\bar{1})$ inclined to the foil surface and is an edge dislocation along $[1\,2\,\bar{1}]$ with $\vec{b} = (a/2)\,[1\,0\,1]$. (b) 60° dislocations along [1 0 1] with $\vec{b} = (a/2)\,[0\,\bar{1}\,1]$ extending on (0 1 0).

dependency of mobile dislocation densities and from the stress index at a stationary creep velocity. The shear strain rate, $\dot{\gamma}$, is expressed by Orowan's equation

$$\dot{\gamma} = \varrho_m \bar{v} b, \tag{2}$$

where ϱ_m is the density of mobile dislocations, $\bar{v}$ their average velocity and b is the magnitude of the Burgers vector. Dislocation velocity, v, is expressed with the effective shear stress, τ_{eff}, and m^* by

$$v = v_0 \tau_{eff}^{m^*} \tag{3}$$

The ratio of τ_{eff} and the applied shear stress τ_{appl} is considered to be constant as the etch pit distribution is always uniform for a given deformation temperature and applied stress. Putting $\dot{\gamma} = \dot{\varepsilon}/S$, S being the Schmid factor, and approximating ϱ_m by

$$\sigma_m = \varrho_0 \sigma^{\zeta} \tag{4}$$

the stress index, m, in Equation 1 can be expressed by

$$m = m^* + \zeta \tag{5}$$

As $m \simeq 3$, m^* can be obtained from the stress dependency of ϱ_m expressed by Equation 4. From the uniform etch pit distribution all dislocations are considered to be mobile. Fig. 10 shows the relation of etch pit density (EPD, ϱ) and shear stress (τ) of the crystal with $n = 1.13$ deformed until stationary creep. In Fig. 10 the relation

$$\tau = \alpha \mu b \varrho^{1/2} \tag{6}$$

is well satisfied, where μ is stiffness factor and α is a constant being nearly 2 in Fig. 10. This relation is verified in various metals and alloys [9] as well as spinel [11] and alumina [18]. As $\varrho_m \propto \tau_{appl}^2$ from Equation 6, ζ in Equation 4 becomes nearly 2. Therefore, the effective stress index m^* of Mn–Zn ferrite crystals is considered to be nearly unity.

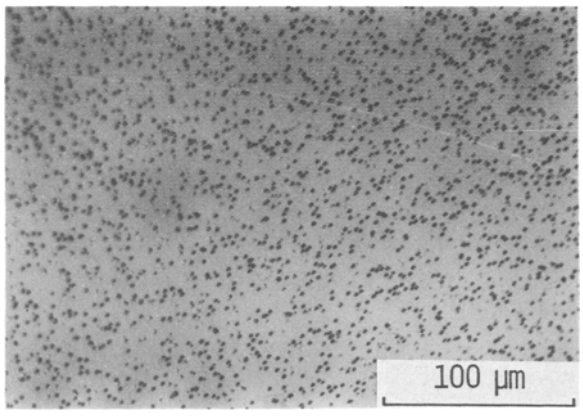

Figure 8 An etch pit pattern of a crystal with $n = 1.13$ deformed at 1250° C along [0 1 1] by compressive creep with 24.5 MPa by 3.01%. The etch pit distribution is almost uniform without cells or subboundaries.

4. Discussions

The deformation parameters, such as stress index, internal stress and effective stress index, and the dislocation configurations, showed that the high temperature deformation of Mn–Zn ferrite crystals is governed by the viscosity ruling for various chemical compositions. Therefore the next problem to be considered are:

(a) what are the obstacles preventing the movement of dislocations and

(b) why the activation energy depends on the composition of the crystal.

The crystals used in the present work were grown in a platinum crucible and the most probable pinning element is platinum. However, as the activation energy depends on the composition, the ions which construct crystals are also considered to pin the dislocations depending on their diffusion constants. The impurities and self diffusions in Mn–Zn ferrite crystals have not been well studied [19], and only the activation energy of the volume diffusion in sintering process is reported to be 4.34 eV [20]. Mn–Zn ferrite crystals have an intermediate spinel structure, and expressing the composition of a non-stoichiometric crystal as

$$Mn_\beta Zn_{1-x-\beta} Fe_{2+x} O_{4+s/2} \tag{7}$$

where $s = \Delta Fe^{3+} + \Delta Mn^{3+}$; the structural formula is expressed as follows:

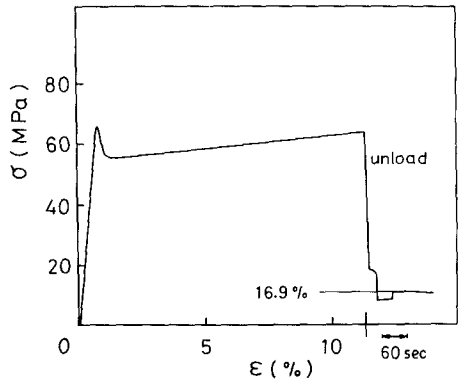

Figure 9 A stress–strain curve for the incremental unloading test to obtain internal stress, σ_i. $n = 1.13$ [0 0 1] 1100° C, $\dot{\varepsilon}_0 = 1.70 \times 10^{-5}\,\mathrm{sec}^{-1}$.

$$[Mn^{2+}_{\beta t'-(1-\alpha)s}Zn^{2+}_{1-x-\beta}Fe^{3+}_{x+(1-t')\beta+\alpha s/8}V_{9(1-\alpha)s/8}]_t$$
$$[Mn^{3+}_{(1-t')\beta+(1-\alpha)s}Fe^{2+}_{x+(1-t')\beta-\alpha s}Fe^{3+}_{2-x-2(1-t')\beta+7\alpha s/8}V_{3(3\alpha-2)s/8}]_o$$
$$O^{2-}_{4+s/2} \qquad (8)$$

where $\alpha/(1-\alpha) = \Delta Fe^{3+}/\Delta Mn^{3+}$, $2/3 \leqslant \alpha \leqslant 1$, $s > 0$, $t' \simeq 0.75$ [21]. V in Formula 8 denotes a vacancy due to the non-stoichiometric construction and the subscript t and o represent the tetrahedral site and octahedral site of a face centred cubic, respectively. In Fig. 11 the atomic ratio of the ions at every site is shown for the compositions used in this work assuming $\alpha = 2/3$ and $t' = 0.75$. As the O^{2-} ions are closely packed in the face centred cubic position, the structural vacancies of positive ions are the dominant point defects [22]. Zn_t^{2+}, Mn_t^{2+}, Mn_o^{3+} and Fe_o^{3+} are at the normal position of spinel structure, but as Fe_t^{3+} and Fe_o^{2+} locate at the inverse sites, the tetrahedral and octahedral sub-lattices around both ions are electrically charged in plus and minus, respectively. The tetrahedral sub-lattices around V_t are also charged in minus. When the composition ratio deviates from $n = 1$, the concentrations of Fe_t^{3+} and V_t increase. Diffusion of positive ions and impurity atoms is impeded by the electrostatic interactions with such negatively charged sub-lattices, while that of O^{2-} is not influenced by the existence of charged sub-lattices. The structural point defects due to the deviation from stoichiometry give rise to lattice distortions and consequently the obstacles for the diffusing positive ions or

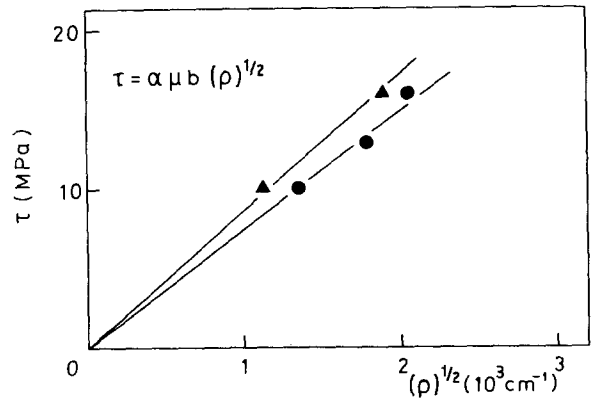

Figure 10 Relation of dislocation densities (etch pit density) and shear stresses in stationary creeps of crystals with $n = 1.13$. $\tau = \alpha\mu b\varrho^{1/2}$. 1253° C (▲) [0 0 1], (●) [0 1 1].

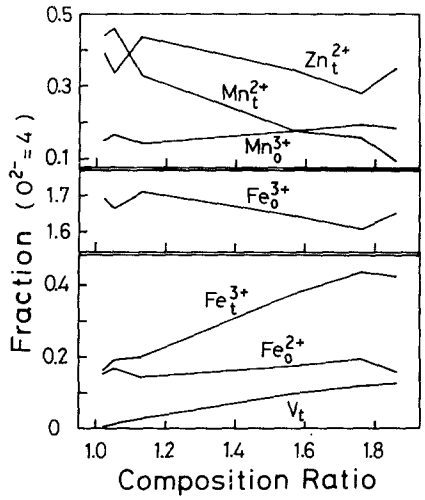

Figure 11 Densities of structural point defects for various chemical compositions of Mn–Zn ferrite crystals.

impurity atoms are introduced. Thus, in Mn–Zn ferrite crystals the positive ions of matrix elements and impurity atoms such as platinum pin the dislocations and the deformation rate of high temperature deformation is governed by the movement of dislocations dragging the atmosphere of pinning ions.

The activation energy of strain velocity varies with the composition of the crystal as in Fig. 5. This can be explained qualitatively considering the structural point defects such as Fe_t^{3+}, Fe_o^{2+} and V_t. They act as obstacles against the diffusion of pinning atoms of ions, and the activation energy varies with the density of obstacles as shown schematically in Fig. 12 for following three cases:

(a) when the density of obstacles is not so high, diffusing atoms can pass through the valleys between the obstacles.

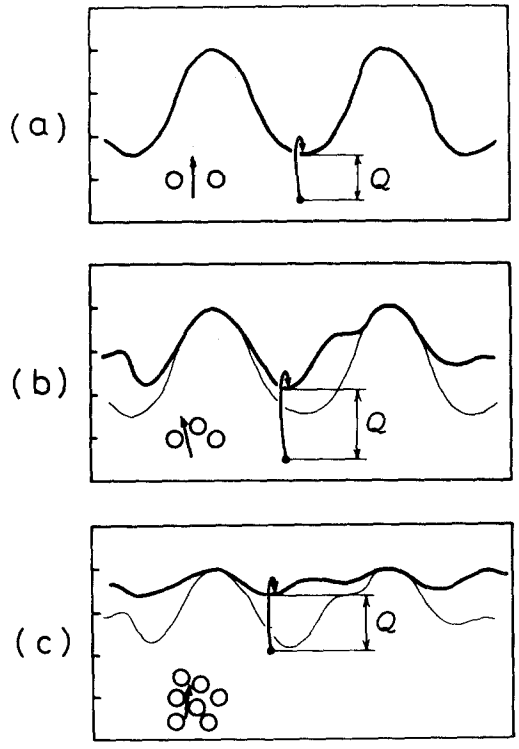

Figure 12 A model to explain the composition dependency of activation energies.

(b) When it becomes high, the tails of neighbouring barriers overlap and consequently the high activation energy is required.

(c) When the composition deviates greatly from stoichiometry and the density of obstacles becomes very high (the number of the structural defects for $n = 1.76$ is nearly 6 in one unit cell), the height of barriers becomes high and almost uniform.

But as the diffusing ions are already in high energy level before passing through the obstacles, the activation energy lowers. Thus the structural point defects due to the deviation from stoichiometry play an important role in the deformation of Mn–Zn ferrite crystals at high temperatures.

Dislocations in Mn–Zn ferrite crystals frequently extend as shown in Fig. 7, however different from spinel crystals [1, 3, 6] the extending plane does not vary along the dislocation line [3, 6] and the climb motion of dislocations is not apparently concerned with deformation [1]. The composition dependencies of activation energies and strain rates in ferrite and spinel crystals are quite dissimilar. Therefore the deformation modes of both crystals are considered to be greatly different from each other. In spinel crystals the activation energy is independent of the composition [3, 23] and the strain rate depends on it [1–3]. This qualitatively agrees with the self-diffusion behaviour of oxygen ions in spinel crystal, that is the pre-exponential term of the self-diffusion constant varies greatly with the chemical composition [24], while its activation energy is almost constant [25]. Therefore, it is considered that the self diffusion of oxygen ions have a great concern with the temperature deformation of spinel crystals. In non-stoichiometric spinel crystals structural defects V_o and Al_t^{3+} exist [26, 27] and the negative charge $3e$ of V_o hinder the diffusion of O^{2-}, however the lattice distortions caused by these defects increase the jumping probability and the pre-exponential term becomes large in non-stoichiometric crystals. As O^{2-} ions diffuse through the thermal equilibrium vacancies in the f c c lattice of oxygen ions, the activation energy does not depend on the chemical composition in spinel crystals.

Finally, the deformation mode at relatively low temperatures (say lower than 1000° C) may be different from the one discussed above. In Fig. 3 it is seen that the inclination of curves (i.e. the activation energies) change at 1000° C for the crystals of $n = 1.05$ [0 0 1] and $n = 1.57$ [0 0 1]. At a lower temperature than 1000° C the activation energy for $n = 1.05$ becomes higher, while that for $n = 1.57$ becomes lower. The deformation mode at a high temperature (1000° C) is explained by the viscous movement of dislocations as discussed above, but the change of activation energy indicates that there exists another activation process in the lower temperature range. The plausible activation process would be the Peierls model. The activation energy in the low temperature is higher for $n = 1.05$ than for $n = 1.57$, and the Peierls potential varies with the chemical composition of the crystal. In the non-stoichiometric crystal the structural positive ion vacancies lower the Peierls potential. This is nearly the same model as is introduced in spinel crystals to explain the change of their slip systems from $\{1\,1\,1\}\langle 1\,\bar{1}\,0\rangle$ to $\{1\,1\,0\}\langle 1\,\bar{1}\,0\rangle$ according to the deviation from the stoichiometric composition [28].

5. Conclusion

The results obtained in this work are summarized as follows:

1. The stress index of strain velocity in stationary creep is nearly 3 and does not depend on the chemical composition of the crystal, while the activation energy varies with it.
2. The deformation parameters and the dislocation configurations observed by TEM and etch pit method revealed that the deformation at a high temperature is governed by the viscous movement of dislocations dragging the atmosphere of pinning atoms or ions.
3. The pinning substances are considered to be the structural defects of positive ions and/or impurity atoms such as platinum, while those of spinel crystals are mostly O^{2-}.
4. The composition dependency of activation energies is explained by considering the structural point defects due to non-stoichiometry such as Fe_t^{3+}, Fe_o^{2+} and the positive ion vacancy, V_t.
5. At temperatures lower than 1000° C crystals deform mostly by Peierls mechanism.

Acknowledgement

The authors thank Messrs. T. Fujimoto and H. Ono for their assistance and Professor H. Fujita, Messrs. K. Yoshida, M. Komatsu and T. Sakata of the Center for Ultra-High Voltage Electron Microscopy of Osaka University for their kind cooperation in using the facilities of the Center. They also express their gratitude to Sanyo Electric Co., Ltd for the supply of the Mn–Zn ferrite single crystals used in this work.

References

1. R. DUCLOS, N. DOUKHAN and B. ESCAIG, *J. Mater. Sci.* **13** (1978) 1740.
2. *Idem, J. Phys. Colloq.* **37** (1978) C7-566.
3. *Idem, Acta Metall.* **30** (1982) 1381.
4. *Idem, J. Phys.* **40** (1979) 381.
5. W. T. DONLON, T. E. MITCHELL and A. W. HEUER, *Phil. Mag.* **45** (1982) 1013.
6. *Idem, ibid.* **40** (1979) 351.
7. P. VEYSSIERE, J. RABIER, H. GAREM and J. GRILHE, *ibid.* **38** (1978) 61.
8. S. KARASHIMA, *Iron and Steel* **65** (1979) 98 (in Japanese).
9. S. TAKEUCHI and A. S. ARGON, *J. Mater. Sci.* **11** (1976) 1542.
10. W. BLUM, *Phys. Status Solidi (b)* **45** (1971) 561.
11. S. MITRA and MACLEAN, *Proc. R. Soc.* **295** (1966) 288.
12. T. HASEGAWA and K. OIKAWA, *Bull. Jpn Inst. Metals* **11** (1972) 192 (in Japanese).
13. H. YOSHINAGA, *ibid.*, **16** (1977) 197 (in Japanese).
14. N. MATSUNO, K. OIKAWA and S. KARASHIMA, *J. Jpn Inst. Metals* **38** (1974) 1071 (in Japanese).
15. H. OIKAWA, J. KARIYA and S. KARASHIMA, *Metal Sci.* **8** (1974) 106.
16. M. UEMURA, T. HYONO, M. UMENO and H. KAWABE, *J. Mater. Sci.* **21** (1986) 2257.
17. M. MIZUSHIMA, *Jpn J. Appl. Phys.* **7** (1968) 893.
18. B. J. PLETKA, T. E. MITCHELL and A. H. HEUER, *J. Amer. Ceram. Soc.* **57** (1974) 388.

19. S. OGAWA and Y. NAKAGAWA, *J. Phys. Soc. Jpn* **23** (1967) 179.
20. G. C. JAIN, K. B. DAS and N. C. GOEL, *J. Amer. Ceram. Soc.* **62** (1979) 79.
21. R. MORINEAU, *Phys. Status Solidi (a)* **38** (1976) 559.
22. P. REIJNEN, *Philips Research Report.* **23** (1968) 151.
23. T. E. MITCHELL, L. HWANG and A. H. HEUER, *J. Mater. Sci.* **11** (1976) 264.
24. K. P. REDDY and A. R. COOPER, *J. Amer. Ceram. Soc.* **64** (1981) 368.
25. K. ANDO and Y. OISHI, *J. Chem. Phys.* **37** (1974) 625.
26. H. JAGODZINSKI and H. SAALFELD, *Zh. Kristallogr.* **110** (1958) 197.
27. H. JAGODZINSKI, *Bull. Soc. Fr. Mineral. Crystallogr.* **90** (1967) 575.
28. M. H. LEWIS, *Phil. Mag.* **17** (1968) 481.

Received 18 June
and accepted 10 July 1985